COMPARISON OF OBSERVATION CORRELATION TECHNIQUES FOR A TELESCOPE SURVEY OF THE GEOSTATIONARY RING

Martin Weigel[(1)], Michael Meinel[(2)], Hauke Fiedler[(1)]

[(1)] *DLR German Space Operations Centre, Münchner Str. 20, 82234 Weßling, Email: martin.weigel@dlr.de*
[(2)] *DLR Simulation and Software Technology, Rutherfordstraße 2, 12489 Berlin*

ABSTRACT

The history of space surveillance by ground based optical telescopes goes back to the early days of spaceflight. Since the beginning, detection of un-catalogued space objects faces the difficulty of initial orbit determination from angles only observations within a limited time period. Multiple short arc data sets have to be combined to calculate orbital elements with sufficient accuracy. For this purpose, the hypotheses have to be tested that one or more short arc measurements belong to the same object. Solving this correlation or object identification problem efficiently becomes more urgent than ever before with the increasing space object population.

The described correlation problem is set up on a large scale by observation simulations for a global network of six robotic telescopes over one month. This survey generates more than 12.000 short arc data sets called tracklets from 1.027 objects in near geostationary orbits (GEO). Initial orbital elements are determined from the short arc measurements applying a circular orbit assumption. Based on the orbital elements, a hypotheses filter for pair and triple tracklet combinations is presented. The newly developed pair filter features high filter rates with simultaneously low filter errors at a negligible computational effort. It is therefore recommended as a pre-filtering stage for more complex correlation methods like recent approaches that utilize the admissible region concept.

1 INTRODUCTION

Surveillance of the geostationary ring requires regular optical observation of active satellites and space debris. Robotic telescope survey is a useful tool to provide frequent measurements and therefore precise position information for a large object population.

There are two different telescope pointing strategies applied during detection of un-catalogued objects. One way is to survey a field of interest in the sky, e.g. in the direction of minimum Sun phase angle, and start follow-on observations as soon as a new object has been detected. The object has to be tracked until the orbit can be determined with sufficient accuracy for a re-identification of the same object in the following night(s). This usually means that the object has to be tracked till the end of the night due to the low information gain connected to the small orbital motion and angles-only measurements. The sampling rate may be lowered with increasing time since first detection, and the telescope may partially resume to the survey task.

An alternative pointing strategy is based on a complete blind sky survey that aims to detect GEO objects multiple times each night by re-observation of pre-defined fields in the sky. In this case, a correct correlation of measurements belonging to the same objects is prerequisite for initial orbit determination. This paper focuses on this correlation step. A method is presented that allows linking short arc angular observations. This difficulty is inherent to all blind survey strategies but also arises during surveys that include follow up observations, since it is often not possible to track an orbit arc of sufficient length, e.g. due to beginning morning twilight at dawn or changing weather conditions.

To avoid correlation of line of sight measurements solely a series of image frames is taken successively and angular rate information is derived. The combination of two topocentric angles and corresponding angular rates forms an augmented measurement that is called tracklet. The task is to test hypotheses that two or more tracklets can be assigned to a single object moving in Earth orbit.

Computationally less expensive correlation techniques may involve analytical orbit propagation, apply a circular orbit assumption or restrict to a single encounter. Due to orbit perturbation errors these simplifications are not valid over a long time. More complex correlation techniques, e.g. following the admissible region concept, impose less restriction and therefore extend the maximum tracklet linkage time.

A representative data set is generated in the first step. Over a period of one month, optical observations are simulated for a global network of six robotic telescopes. In the second step, the performance of a simple but light-weight correlation technique is analysed and compared to some methods presented recently.

2 OBSERVATION SIMULATION

As a good assumption, the distribution of space debris follows the orbital distribution of known space objects. The publically available Two-Line Elements (TLE) may serve as a seeding element for the generation of a simulation population. The TLE catalogue with date 2010-11-03 was filtered for all objects with a perigee height above 30.000km and an apogee height below 50.000km. A total number of 1027 object passed this "near GEO" filter. The authors had access to a dump file of the ESA DISCOS database that records a principal radius for a subset of 972 objects. Applying a spherical shape model a projected surface area is computed from the radius. For the 55 objects without radius from DISCOS file a normal random number was assigned to the effective surface. In addition random numbers were generated for the mass and solar radiation pressure coefficients of all objects. Random numbers follow a normal distribution and satisfy the limits from Tab. 1.

Table 1: Object Property Limits

Object Mass	500kg – 5000kg
Solar Radiation Pressure Cross Section	5m² - 500m²
Solar Radiation Pressure Coefficient	0.5 - 2.5

The TLE data are propagated to a common epoch and transformed to osculating state vectors. Orbits are numerically integrated during the simulation time form 2011-12-01 to 2011-12-31. The orbit model comprises spherical harmonics of the Earth gravity field up to degree and order of six, solar radiation pressure computed by a simple cannonball model and third body attractions by the Sun and the Moon.

2.1 Global Telescope Network

The entire GEO ring can principally be covered by three telescope sites separated uniformly in longitude around the Earth at latitudes between ±20° to ±40°. A pair wise configuration of telescopes on the northern and southern hemisphere further improves observation geometry, independent weather conditions as well as observation frequency. Thus, the simulation includes three telescope pairs with data from Tab. 2.

Table 2: Sensor Sites & Observation Night Probability

A) Parque Natural Sierra de San Pedro Martir, Mexico	80%
B) Zimmerwald Observatory, Swiss	40%
C) Okayama Astrophysical Observatory, Japan	40%
D) La Silla Observatory, Chile	80%
E) South African Astronomical Observatory	80%
F) Siding Spring Observatory, Australia	80%

If a random generated number exceeds the probability value no measurements are taken by the telescope for the specific simulation night. This simple availability model reflects weather conditions and sensor outages. The telescope parameters are listed in Tab. 3. The reference magnitude is 15.7^{mag} for a sphere with diameter of 1m and albedo of 0.2 at a reference distance of 36.000km.

The "CCD Equation" is used to compute the signal-to-noise ratio (SNR) for all measurements made [1]:

$$SNR = \frac{S}{\sqrt{S + n_{PIX}\left(N_{READOUT}^2 + N_{DARK} \cdot t_{int} + N_{BACK}\right)}} \quad (1)$$

where S is the Signal in electrons, $N_{READOUT}$ is the frame readout noise in electrons per pixel, N_{DARK} is the dark current noise as electrons per pixel and second and term N_{BACK} summarizes all sources of background noise. The number of illuminated CCD pixel n_{PIX} is calculated from the object trail on the frame. It is assumed, that the trail width is equal to the full width at half maximum (FWHM) and the trail length is defined by the angular velocity in sensor frame. Object detection is possible if the computed SNR exceed a minimum value.

Table 3: Telescope Parameter

Aperture Diameter	30cm	Readout Noise	5.74 e/pixel
Field of View	2° x 2°	Dark Current	3.0 e/pixel/s
Pixel	4096 x 4096	Sky Background	18^{mag}
FWHM	4.1"	Quantum Efficiency	0.6
Integration Time	8s	Optical Transmission	0.7
Readout-Time	16s	Minimum SNR	4

2.2 Survey Strategy

Scanning declination stripes in the sky is a common survey strategy to cover objects in inclined orbits [2], [3]. Successive frames are taken at the same field in the sky to proof object detection and obtain a series of line of sight measurements. After a series of frames the telescope is pointed to a neighbouring field without overlap by increasing or decreasing the declination angle by the field of view size. This procedure continues till a strip of constant right- ascension is covered. The population's distribution in inclination supports a maximum and minimum declination limit of ±15°. Moreover, the distinct distribution of the right-ascension of the ascending nodes allows reducing the stripe's declination extension when the centre declination δ_0 varies as a function of right-ascenion α according to:

$$(2) \qquad \delta_0 = 7.5° \cdot \sin(\alpha + 8°)$$

Fig 1. illustrates the shifting stripe centre line. Four survey fields above and below the centre line are required to survey the declination band with a relative high spatial density. Coverage of the most frequent orbits with near zero inclination is ensured even for the most elongated stripes.
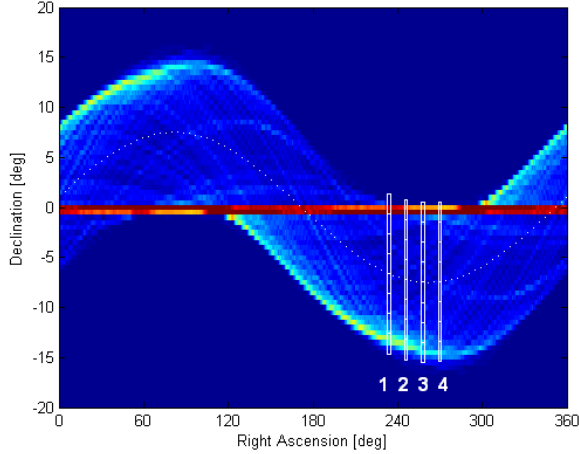
Figure 1: Population Spatial Density, Declination Stripe Centre Line (dashed white) & Survey Fields of 4 example Stripes (white)

Recalling the integration and read-out times from Tab. 3, and assuming that slewing the telescope is always finished within the frame readout time, it takes 16 minutes to scan one declination stripe of 8 survey fields and 5 frames per field. In this time, a perfect GEO object moves 4° along the orbit. Immediate re-observations would span a relative small orbital arc. On the other hand, longer latency is connected to a larger sun phase angle, since there is a minimum time once every night. The interests for a large orbital arc and high detectability are balanced in the following way. The declination stripe with the same right-ascension is scanned two more times. For re-observation of the same objects the right-ascension is then increased by 12° and the centre declination is adjusted before the three "parallel" stripes are scanned for a second time. This repeats for a third and fourth time with the purpose to obtain up to four tracklets per object in one night. The described stripe pattern is shown in Fig 1. Referring to the numbering introduced there the stripe sequence is 111-222-333-444.

It takes 196 minutes to finish the 12 stripe pattern. The pattern is repeated multiple times during one observation night. Any shorter patterns with fewer stripes can be realized in the remaining night time, e.g. "2 parallel stripes with 2 re-observations" down to a single stripe at minimum. Shorter stripe patterns are also scheduled to avoid Earth eclipse.

The blind survey is scheduled in the following steps:

- Calculating night start and end times defined by the condition of a maximum Sun elevation of -12°.

- Timely and spatial sampling of all possible survey stripes per observation night and telescope.

- Observation constrains are checked at the field edges. All stripes are ruled out that violet one of these:

    A) Pointing elevation < 20°,

    B) 10° < Sun phase angle < 90°,

    C) Moon exclusion angle between 0.56° and 20° depending linearly on moon phase.

- Starting at dusk and in every second night at dawn the best stripe pattern are successively selected. The applied criterion is the linear combination of:

    A) Mean time since last stripe observations,

    B) Mean Sun phase angle to increase detectability,

    C) Orbit arc length inherent to the pattern.

After the survey stripes and field are scheduled for every telescope and every observation night, observations are simulated for all population object. For simplicity all aspects of image generation and processing, like looses due to star trails, bright stars, cosmic rays, linking object on frames etc., are modelled by an astrometric data reduction probability of 70 % per frame. If three out of five detections are successful the measurement data are computed (tracklet probability 83.7%). Measurement errors are introduced to the single topocentric angles as a Gaussian distributed random number of 0.2" (1σ) and 2.3" (1σ) to bias all measurement from one tracklet.

In the course of the one month survey 36.840 survey fields are scheduled for all six telescopes, resulting in 16.431 simulated tracklets without application of the astrometric reduction probability or detection constraints. With these limitations the measurement data set is reduced to 12.608 tracklets. In total 906 out of 1027 objects are spatially and timely covered by the one month survey, 121 are missed. Application of data reduction success probability and of detection limits leads to a further lose of 65 objects. Therefore, the major limiting factor is the survey spatial and temporary coverage.

The telescopes on the northern hemisphere discover around half of the objects which are geometrically visible from their site. The sensors on the southern hemisphere detect less, due to shorter night times in December. Also visible from the data are the assigned values of sensor availability.

3 HYPOHTESES FILTERING

A newly discovered object can enter the catalogue database if the orbit is determined with sufficient accuracy to be reliably distinguished from orbital data and observations of other objects. This surely requires a certain number of tracklet measurements over a time period of multiple days. For any set containing n elements, the number m of distinct k-element subsets is calculated by the binomial coefficient:

$$(3) \qquad m(n,k) = \binom{n}{k} = \frac{n!}{k!(n-k)!}$$

Because of the large pool of uncorrelated tracklets, $n = 12604$ in case the catalogue is build up from scratch, the number of hypotheses quickly exceeds the number of combinations that can be tested for a growing value k. It is therefore important to filter out wrong hypotheses comprising few tracklets ($k = 2, 3, ...$) very effectively and thereby reducing the number of hypotheses incorporating more tracklets. Starting with a circular orbit determination from single tracklets a minimum number of computations is required ($m = n$ for $k = 1$). Based on the circular orbit elements pair hypotheses (for the data set $m(12604,2) \approx 7.9 \cdot 10^7$) will be filtered and triplet hypotheses ($m(12604,3) \approx 3.3 \cdot 10^{11}$) will be tested by further linking of pair filtering results.

3.1 Circular Orbit Determination

In theory three line of sight measurements and the corresponding time stamps are sufficient to calculate one or more orbit solutions in the form of a full six-dimensional state vector. In practice tracklets containing even more than three line of sight measurements hold information on two angles and the corresponding angular rates. Angular accelerations can not be observed during the small time interval of a few minutes and are missing for a full six element orbit determination. A circular orbit is described by four elements, eccentricity is zero and the argument of perigee is not defined. By application of a circular orbit assumption an initial orbit can be computed from single tracklets and the subsequent filtering of a much larger number of hypotheses is basically a comparison of orbital elements.

In [4] a circular orbit determination method is formulated as a root search of a non-linear function of semi-major axis. The function is the difference between two terms to dynamically and geometrically calculate the angle between two inertial position vectors corresponding to two line of sight measurements. The first and last tracklet line of sight measurements should be used as input since they have the largest time separation.

To incorporate all line of sight information of the tracklet, an alternative iteration scheme is presented here. First, a least-square fit is performed for both angles to obtain a linear function with the lowest RMS measurement residuals. Afterwards a Newton-Iteration of semi-major axis a is started based on the difference in inertial speed v calculated from observations and dynamics:

$$a_{i+1} = a_i + \left(v_{dyn} - v_{obs} \right) \bigg/ \left(\frac{\partial v_{dyn}}{\partial a} - \frac{\partial v_{obs}}{\partial a} \right). \qquad (4)$$

The circular orbit dynamics state that:

$$v_{dyn} = \sqrt{\frac{GM}{a}}, \qquad \frac{\partial v_{dyn}}{\partial a} = -\frac{1}{2} \cdot \sqrt{\frac{GM}{a^3}}. \qquad (5)$$

The observed speed in inertial frame follows from derivation of the position vector with respect to time:

$$v_{obs} = \left| \frac{\partial \bar{r}}{\partial t} \right| = \left| \frac{\partial(\bar{R} + d \cdot \bar{e})}{\partial t} \right| = \left| \frac{\partial \bar{R}}{\partial t} + \frac{\partial d}{\partial t} \cdot \bar{e} + d \cdot \frac{\partial \bar{e}}{\partial t} \right|. \qquad (6)$$

with the sensor position in inertial frame $\bar{R}$, the line of sight vector $\bar{e}$ and their time derivatives are evaluated at a common epoch, e.g. at half time between first and last measurement point and d being the topocentric distance. The partial derivative of the observed speed with respect to semi-major axis is given by:

$$\frac{\partial v_{obs}}{\partial a} = \frac{1}{v_{obs}} \cdot \left[\left(\frac{\partial \bar{R}}{\partial t} + \frac{\partial d}{\partial t} \cdot \bar{e} + d \cdot \frac{\partial \bar{e}}{\partial t} \right) \cdot \right.$$
$$\left. \left(\frac{\partial}{\partial a} \left(\frac{\partial d}{\partial t} \right) \cdot \bar{e} + \frac{\partial d}{\partial a} \frac{\partial \bar{e}}{\partial t} \right) \right]. \qquad (7)$$

Squaring the equation of the position vector $\bar{r} = \bar{R} + d \cdot \bar{e}$ and solving the resulting quadratic equation for range the solution can be found as [4]:

$$d = -\bar{R} \cdot \bar{e} + \sqrt{\left(\bar{R} \cdot \bar{e} \right)^2 - \left| \bar{R} \right|^2 + a^2}. \qquad (8)$$

From Eq. 8 the missing terms for range rate and the partial derivatives with respect to semi-major axis are computed as:

$$\frac{\partial d}{\partial t} = -\left(\frac{\partial \bar{R}}{\partial t} \cdot \bar{e} + \bar{R} \cdot \frac{\partial \bar{e}}{\partial t} \right) +$$
$$\frac{\left(\bar{R} \cdot \bar{e} \right) \cdot \left(\frac{\partial \bar{R}}{\partial t} \cdot \bar{e} + \bar{R} \cdot \frac{\partial \bar{e}}{\partial t} \right) - \left(\bar{R} \cdot \frac{\partial \bar{R}}{\partial t} \right)}{\sqrt{\left(\bar{R} \cdot \bar{e} \right)^2 - \left| \bar{R} \right|^2 + a^2}}, \qquad (9)$$

$$\frac{\partial d}{\partial a} = \frac{a}{\sqrt{\left(\bar{R} \cdot \bar{e} \right)^2 - \left| \bar{R} \right|^2 + a^2}}, \qquad (10)$$

$$(11) \quad \frac{\partial}{\partial a}\left(\frac{\partial d}{\partial t}\right) = \frac{-a \cdot \left[\left(\overline{R} \cdot \overline{e}\right) \cdot \left(\frac{\partial \overline{R}}{\partial t} \cdot \overline{e} + \overline{R} \cdot \frac{\partial \overline{e}}{\partial t}\right) - \left(\overline{R} \cdot \frac{\partial \overline{R}}{\partial t}\right)\right]}{\sqrt{\left[\left(\overline{R} \cdot \overline{e}\right)^2 - \left|\overline{R}\right|^2 + a^2\right]^3}}$$

The initial value is always the semi-major axis of the geostationary orbit. After iterative improvement up to a certain convergence limit the missing orbital elements inclination, right-ascension of ascending node and true longitude can easily be computed [4].

An assessment of the circular orbit determination method described in [4] for two line of sights ("2 LOS") and the method presented above for an arbitrary number of line of sights ("≥2 LOS") is performed from all tracklets by comparison of the determined orbital elements against the reference elements of simulation input. Orientation of the orbital plane is described by the elements inclination and right ascension of ascending node. The second is hardly defined for near zero inclinations and RAAN thresholds can easily be violated. To avoid this, the term $\Omega \cdot \sin i$ is used instead. As can be seen from Tab. 4 both methods lead to comparable errors in the orbital plane orientation. On an overall view, standard deviation of semi-major axis error is larger for the second method with an arbitrary number of line of sight measurements. Further investigations revealed that this is not the case for low inclinations where this method lead to lower semi-major axis errors compared to method from literature [4]. A combination of both methods is therefore applied. A first circular orbit is determined with the new method, if the resulting inclination exceeds 7° a second iteration is performed based on the old method. This combination results in overall slightly lower errors.

Table 4: Circular Orbit Determination Error (STD)

Method	Semi-major Axis	Inclination	RAAN sin(incl)
"2 LOS"	1142 km	0.356°	17.818°
"≥2 LOS"	2661 km	0.361°	17.255°
COMBI	1128 km	0.356°	17.807°

3.2 Tracklet Pair Filter

Before the actual filtering of tracklet pair hypotheses all combinations of simultaneous sensor measurements can be excluded. This step is just necessary when the measurement data handling does not include information on simulations object observations with the same telescope. All tracklet pairs are ruled out that originate from the same sensor and same images, or originate from the same sensor and overlap in time respectively. The simulation data contain 12.672 pairs of such multiple objects observations. This is a very small fraction of all possible tracklet pair combinations.

The circular orbit determination provides four orbital elements that could be exploited to filter hypotheses. The four elements are again semi-major axis, inclination, right ascension of ascending node (RAAN), and true anomaly. Due to RAAN singularity at zero inclination, the product of RAAN and the sine of inclination is used as well as the true longitude being the sum of RAAN and the true anomaly. The true longitude changes over time and propagated to a common comparison time. The true longitude of the first tracklet is propagated forward to half time between both tracklets, and the true longitude of the second tracklet is propagated backwards to the same point.

The standard deviation of the differences in the four quantities is computed for all true pair hypotheses. The 1-sigma errors are multiplied by a varying scaling factor to derive a set of filter thresholds. All pair hypotheses are then tested against the set of thresholds. Hypotheses are filtered out if the absolute difference of the orbital elements exceeds the threshold. By variation of the filter thresholds scaling factor the filter characteristic is obtained, see Fig 2. The filter rate is the fraction of excluded false pair hypotheses to the total number of false hypotheses and the filter error is the fraction of wrongly removed true pair hypotheses to the total number of true hypotheses.

The linear filter characteristic for semi-major axis is equivalent to zero filter performance since the ratio of true to false hypotheses removed stays constant. The filter based on the difference in inclination and RAAN multiplied with the sine of inclination perform both comparable well. Around 60% to 70% of all false pairs can be precluded before the filter error starts to increasingly rise. The maximum time difference between both tracklets was set to 12 hours, meaning that observations of most combinations are taken within one observation night. For this time difference true and false pair hypotheses can easily be distinguished by a comparison of propagated true longitude.
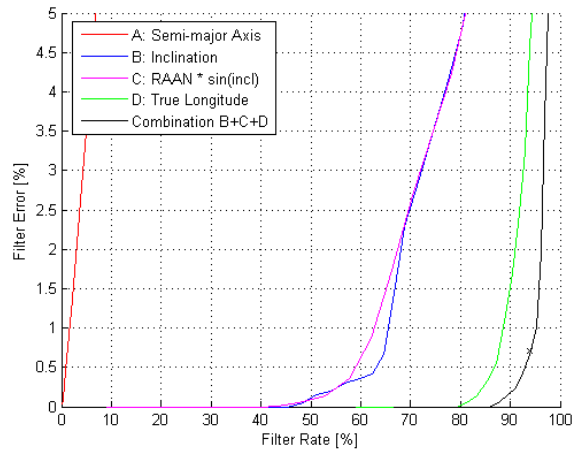
Figure 2: Individual and combined filter performance

Most efficient is a combined filter of differences in orbital plane orientation and true longitudes. The single element thresholds are equally weighted, meaning that the previously calculated 1-sigma errors are always scaled with the same factor. By violation of at least one threshold, the tracklet pair is filtered out. A filter rate of up to 95% is achieved at a filter error of approximately 1%. Note that from the simulation data the number of false pair hypotheses exceeds the number of true hypotheses by a factor of around 500.

As already indicated the performance of the true longitude filter depends on the time difference between the two tracklets. This is due to the errors in semi-major axis determinations, a mean motion errors respectively, and the accumulating error over propagation time. The difference in orbital plane orientation is nearly time invariant. More important, the orbital plane is determined more precisely for longer time interval between the first and last tracklet measurement. This time span varies because of the astrometric data reduction probability of each frame. A pair of tracklets can have different arc lengths and depend on the minimum value the different thresholds are applied for the orbital plane orientation.

The actual filter thresholds should be selected at a point where a moderate gain in filter rate is connected to an unjustifiable large increasing filter error. In Fig. 2 this point is located at a filter error of 0.5% to 1%. Consequently the scaling factors of the neighbouring filter thresholds to the 0.5% filter error are linearly interpolated. The interpolated scaling factor is applied to the 1-sigma errors of all elements to obtain single element thresholds. The combined filter presents a slightly larger filter rate and a higher filter error than 0.5%. The same interpolation is repeated for every additional day of tracklet time separation and for different minimum value of tracklet arc length. Interpolation results are plotted in Fig. 3.
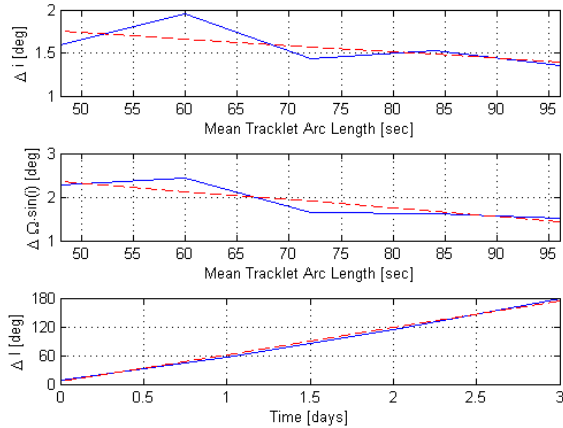
Figure 3: Interpolated filter thresholds (blue) and linear fits (red)

A tendency for larger threshold can be recognized for both elements describing the orbital plane orientation. At a time interval of three days the thresholds for the difference in the propagated true longitudes reach the value of 180°, which is the limit to distinguish between short and long arc solutions. The final filter settings follow from a linear fit to the three filter threshold curves:

$$\Delta i = 2.128° - 0.0077° \cdot s^{-1} \qquad (12)$$

$$\Delta(\Omega \cdot \sin i) = 3.285° - 0.193° \cdot s^{-1} \qquad (13)$$

$$\Delta l_{prop} = 4.932° + 56.43° \cdot d^{-1} \qquad (14)$$

Combined application of the singe element thresholds results in the filter performance shown in Fig. 4. Starting with tracklet from one observation night a filter rate of more than 93% constantly falls till a tracklet time separation of around three days. For longer time intervals the filter rate stays at a constant level between 70% and 75%. The filter error ranges between 1% - 2% for tracklet time difference of up to 17 days and between 2% - 4% for more days.
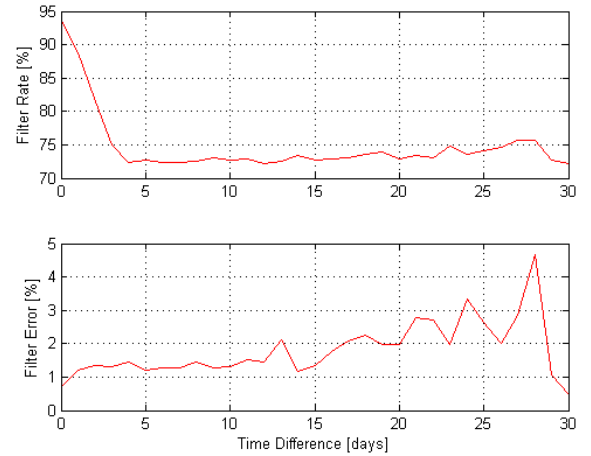
Figure 4: Combined pair filter performance

Recalling the influence of the tracklet arc length on the orbit plane determination, there may be the possibility to increase accuracy by a joint circular determination from two tracklets. The iteration method based on two line of sight measurements can easily be adapted to handle long and short arc solutions as well as multiple encounters. One line of sight measurement from each tracklet is sufficient input that covers a much larger tracking arc. True and false pair hypotheses may be distinguished by the distance of the remaining line of sight measurement from the newly found orbit. For all pair hypotheses that passed the original filter a second circular orbit based on both tracklets was computed test wise. The RMS error of the remaining line of sights did not allow filtering out further false hypotheses. The RMS errors were analysed depending on the tracklet arc length.

3.3 Tracklet Triple Filter

A tracklet triple hypothesis is inherently associated to three pair hypotheses. All triple combinations may therefore be evaluated by the filter results already computed for the corresponding pair hypotheses. In the following it will be required that all three tracklet pair combinations passed the pair filter to support the corresponding triple hypotheses. As an example, for a pair filter rate of 80% and a pair filter error of 2% one would expect a triple filter rate of $1-(1-0.8)^3 = 99.2\%$ and a triple filter error of $1-(1-0.02)^3 = 5.88\%$.

All triple combinations contained within the simulation data set are tested and the obtained triple filter performance is given in Fig 5. The filter rate reaches more than 99% for observations within one night and falls to a relative constant level of nearly 95% after a time separation of 10 days between first and third tracklet measurement. This is in line with the expectations from the pair filter performance given in Fig. 4. The longer time difference till constant level of filter rate can be explained by the longer time interval covered by three observations. The filter errors are much larger than expected. Only a minority of true triple tracklet hypotheses could enter a further processing step. One explanation may be that the linked pair hypotheses may not be as independent as assumed.

Further investigation will focus on two more questions. How does the filter rate and filter error evolves if two of tree pair hypotheses have to be confirmed, e.g. the pair of the first and second tracklet and the pair of second and third tracklet. Second is it possible to utilize the more precise circular orbits from a tracklet pair for filtering triple tracklet hypotheses.
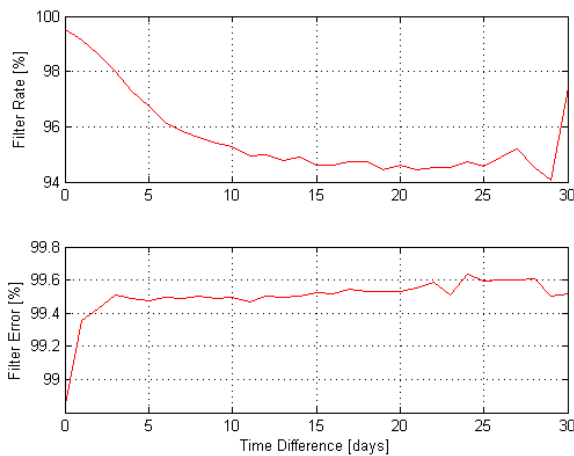
Figure 5: Linked triple filter performance

4 COMPARISON TO OTHER MEHTODS

The following discussion is a qualitative comparison to some published results of alternative methods.

Milani et al. [5] introduced the admissible region concept. The missing tracklet observations in range and range rate are restricted by physical constrains like an elliptic orbit assumption or minimum distance. Tommei et al. further developed this concept for Earth orbiting satellites [6]. An infinite number of orbit solutions are contained within the admissible region but only a few are inside the measurement accuracy of a second tracklet. Common to all methods published recently is the propagation of many discretization points inside the admissible region. This mostly includes propagation of covariance information or probability density function to compute a probability distance to the second tracklet measurements. The distance metric of the best solution found is tested against a threshold to allow data association.

The correlation results are promising, e.g. in [7] a filter rate of 85% at a filter error of 0.5% was obtained for a maximum time separation of 26 hours and for the more easy case of 11 objects in clearly different orbits (GEO, MEO, eccentric MEO, etc.). From the same data triple tracklet combinations are filtered with a rate of 98.5% and a filter error of 0.7% by gating pair filter results.

To limit the number of discretization points an adaptive grid refinement [7] or a search on iso-energy-grid [8] may be applied. Still, hundreds of sampling points have to be propagated and thousands of loss function calls have to be made. The computational burdens limit the number of pair hypotheses that can be tested to less than ten in one second on a modern personal computer [7].

In [3] catalogue correlation in performed with real observations and in an operational environment. A least square circular orbit determination is performed from all combinations of tracklets that could not be assigned to a catalogue object in a first step. Orbits with a residual RMS error lower than 2" are kept as candidate orbits. Next step is the comparison of orbital elements of a candidate orbit and all catalogue orbits for the purpose to assign the tracklet pair to a known object. For the remaining single tracklets a circular orbit is computed and a correlation with catalogued orbits and candidate orbits is tested. Depending on which types of orbit are compared different orbital elements are used, e.g. filtering single tracklets is solely based on inclination.

5 CONCLUSIONS

In this paper, a large scale correlation task is set up by simulation of 12.604 tracklet observations from 1.027 objects in near geostationary orbits. Inital orbital elements are determined from the short arc data sets using a circular orbit assumption. A novel iteration scheme for semi-major axis is presented. Based on the orbital elements, a hypotheses filter for pair and triple combination of short arc measurement data is developed. The new tracklet pair filter features high

filter rates with simultaneous low filter errors at a negligible computational effort.

From the results published in literature it may not be possible to correlated all tracklets for a telescope network with the existing correlation methods, since the pool of uncorrelated observations growth and more prominent the number of pair combinations. Even with massive a parallelization the computation may not be finished within a reasonable time. Single tracklet filtering may have to be applied as a first correlation step and should include the comparison additional orbital elements.

6   REFERENCES

1. Howell, S.B. (2006). *Handbook of CCD Astronomy*. Cambridge University Press., Cambridge, UK, pp73.

2. Schildknecht T. (2007). Optical Survey for Space Debris. *Astron. Astrophys. Rev.* 14, 41-111.

3. Herzog J. (2010), Build-up and Maintenance of a Catalogue of GEO Objects with ZimSMART and ZimSMART 2. In *Proc. 10th International Astronautical Congress,* IAC-10.A6.5.2

4. Beutler, G. (2004). *Methods of Celestial Mechanics – Volume I*. Astronomy and Astrophysics Library, Stringer, pp369-373.

5. Milani, A., Gronchi, G., Vitturi, M.D.M. & Knezevic Z. (2004) Orbit Determination with Very Short Arcs. I Admissible Regions. *Celestial Mechanics and Dynamical Astronomy*, Vol. 90, 57–85.

6. Tommei, G., Milani A. & Rossi A. (2007) Orbit Determination of Space Debris: Admissible Regions. *Celestial Mechanics and Dynamical Astronomy*, Vol. 97, 289–304.

7. Gadaleta, S.M., Horwood, J.T. & Poore A.B. (2012). Short Arc Gating in Multiple Hypothesis Tracking for Space Surveillance. In *Proc. SPIE 8385, Sensors and Systems for Space Applications V.*

8. Siminski J.A., Montenbruck O., Fiedler H. & Weigel M. (2013). Best Hypotheses Search on Iso-Energy-Grid for Initial Orbit Determination and Track Association. *23rd AAS/AIAA Spaceflight Mechanics Meeting*.